Thin Solid Films 629 (2017) 97–102

Contents lists available at ScienceDirect

Thin Solid Films

journal homepage: www.elsevier.com/locate/tsf

Oxygen diffusion in TiO_2 films studied by electron and ion Rutherford backscattering

G.G. Marmitt[a,*], S.K. Nandi[b], D.K. Venkatachalam[b], R.G. Elliman[b], M. Vos[b,c], P.L. Grande[a]

[a] Instituto de Física, Universidade Federal do Rio Grande do Sul, Porto Alegre, RS, Brazil
[b] Department of Electronic Materials Engineering, Research School of Physics and Engineering, The Australian National University, Canberra, Australia
[c] Atomic and Molecular Physics Laboratories, Research School of Physics and Engineering, Australian National University, Canberra, Australia

ARTICLE INFO

Article history:
Received 24 October 2016
Received in revised form 23 February 2017
Accepted 12 March 2017
Available online 18 March 2017

Keywords:
Diffusion
RBS
Electron-RBS

ABSTRACT

The diffusivity of oxygen in thin, sputter-deposited TiO_2 films, as can be used in RRAMs, is measured using electron and ion backscattering techniques. The as-grown sample consisted of two layers ($Ti^{16}O_2$ and $Ti^{18}O_2$) and was annealed between 500 °C and 900 °C. The depth profiles of ^{18}O, as measured with both techniques, were similar. The extent of diffusion was much larger than expected from the literature data for O diffusion in single-crystal rutile, suggesting that defects in the sputter-deposited film play an essential role in the diffusion process.

1. Introduction

Oxygen diffusion in rutile single crystals has been investigated extensively in the past [1–6]. TiO_2 has many technological applications but many of these exploit an amorphous or polycrystalline phase [7]. To our knowledge no data exist for oxygen diffusion under these conditions. In particular, TiO_2 is a prototypical memristive material [8], used for resistive random access memory (RRAM). The resistive switching is a consequence of the formation (and destruction) of oxygen-deficient filaments in the TiO_2 layer by electric-field induced diffusion of oxygen [8]. Details of these processes are still poorly understood, but it is clear that O diffusion is an essential ingredient. Here we study O self-diffusion during the annealing of sputter-deposited thin films.

Different experimental techniques have been used in the literature to determined the diffusivity and activation energy for oxygen self-diffusion in TiO_2, which include mass spectrometry and nuclear reaction analysis by ^{18}O labeling. They were successfully used for the cases where the diffusion length is several hundreds of nm. For much shorter diffusion lengths a new technique was proposed recently [9], using the difference in energy of keV electrons scattered elastically from either ^{18}O or ^{16}O. This technique, electron Rutherford backscattering spectrometry (ERBS) has depth-sensitivity based on the electron inelastic mean free path (IMFP). Therefore electrons scattered from ^{18}O (or ^{16}O) atoms close to the surface are more likely to contribute to the elastic peak than those scattered from O further below. In contrast ion scattering provides information about the depth distribution based on the energy loss per unit length traveled. Here we compare the results from both approaches.

2. ERBS technique

Fast electrons moving through matter interact with nuclei (subsequently referred to as atoms) and electrons. Elastic collision between a fast electron and an atom transfers momentum q, and hence energy to the scattering atom. If the atom is initially at rest it acquires a kinetic energy $q^2/2M_i$, where M_i is the mass of atom i. However, if the impacted atom has a momentum p before the collision (e.g. due to thermal vibrations), then the recoil energy transferred to this atom is Doppler broadened and given by

$$E^i_{rec} = \frac{(p+q)^2}{2M_i} - \frac{p^2}{2M_i} = \frac{q^2}{2M_i} + \frac{p\cdot q}{M_i}. \quad (1)$$

The electron loses this amount of energy. If the target contains atoms with different masses M_i, then the elastic peak will split up into several components with energies related to their mass. Under our experimental conditions almost all detected electrons have linear trajectories with a single large-angle backscattering collision occurring at depth x. In a previous work about multiple scattering in

* Corresponding author.
E-mail address: gabriel.marmitt@ufrgs.br (G. Marmitt).

http://dx.doi.org/10.1016/j.tsf.2017.03.024
0040-6090/

ERBS experiments, we have shown that such approximation allows for the determination of the stoichiometry of TiO_2 films within a 1–2% error margin [10]. For isotropic materials the width due to thermal motion of each component is given by

$$\sigma_i = \sqrt{\frac{4}{3}\bar{E}^i_{rec}\bar{E}^i_{kin}}. \quad (2)$$

with $\bar{E}^i_{rec}$ the mean recoil energy ($q^2/2M_i$) and $\bar{E}^i_{kin}$ the mean kinetic energy of atom i [11].

The electron may also scatter inelastically, i.e. create electronic excitations but then the energy loss is generally so large that it will not contribute to the elastic peak. It is commonly assumed that the electron does not change its direction in inelastic events and hence the shape of a trajectory is determined by elastic collisions. The probability that a trajectory contributes to the elastic peak is determined by the likelihood that no inelastic scattering occurred. If I_0 is the number of electrons backscattered from each depth, then their contribution to the elastic peak will vary as

$$I(x) = I_0 e^{-l(x)/\lambda}, \quad (3)$$

where $l(x) = x(1/\cos(\theta_1) + 1/\cos(\theta_2))$ is the length traveled and λ is the IMFP of electrons with energy E_0 and $\theta_{1,2}$ the incoming and outgoing angles.

When a substrate is covered homogeneously by an overlayer then the ratio of the overlayer and substrate signal strength is a measure of the overlayer thickness [12]. Similarly, when the material has a concentration depth profile $\phi^i(x)$ for some element i, the peak intensity of element I as measured by ERBS is proportional to

$$H^i = \sigma^i \int_0^\infty I(x)\phi^i(x)dx, \quad (4)$$

where σ^i is the differential cross section for backscattering from element i. Because only the ratio of peak intensities is measured we cannot uniquely determine $\phi^i(x)$, so further assumptions about the depth profile are necessary. A typical assumption is that atomic distributions can be described as diffusion profiles as calculated from the diffusion equation

$$\frac{\partial\phi^i}{\partial t} = D\nabla^2\phi^i, \quad (5)$$

where D is the diffusion coefficient. The oxygen isotopes have similar chemical properties, thus the diffusion coefficient is considered independent of variations of only one isotope concentration. It has already been shown [9] that solutions with different diffusion coefficients lead to different measured peak intensity ratios.

3. Experimental procedure

In order to study O diffusion in TiO_2, two sets of samples were prepared. Set A consisted of pieces of a Si wafer on which 60 nm of $Ti^{16}O_2$ was first deposited followed by 20 nm of $Ti^{18}O_2$. Set B had the isotope composition inverted: 60 nm of $Ti^{18}O_2$ followed by 20 nm of $Ti^{16}O_2$. We also grew samples with a single, isotopically-pure TiO_2 layer with 80 nm thickness. The reactive sputter depositions were performed with a Ti metal target and oxygen containing ambient, which was powered by a pulsed DC source at 5 kHz and pulse length of 0.4 µs. The system used was calibrated for a deposition rate of 0.67 Å/s, which for our samples leads to total deposition times of about 1000 s. The samples' temperature during deposition remained below 200 °C. The $Ti^{18}O_2$ layers were grown using 99.9% pure $^{18}O_2$ gas during deposition.

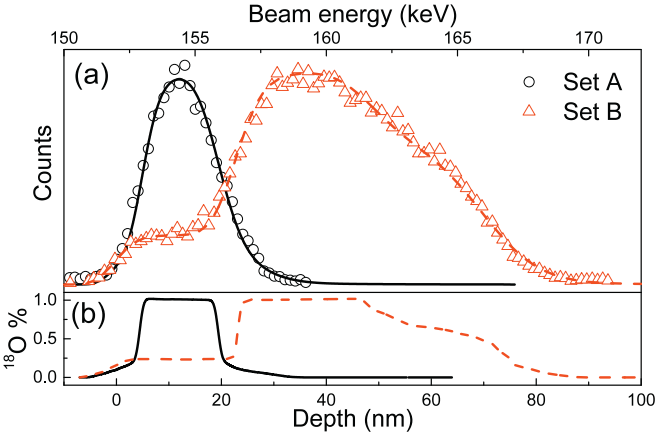

Fig. 1. (a) NRP spectra obtained using the 151 keV resonance in the $^{18}O(p,\alpha)^{15}N$ reaction for both sets. The lines are simulated intensities based on the $^{18}O_2$ depth profile shown in (b).

Nuclear Reaction Profiling (NRP) was used to measure the ^{18}O depth profile using the ^{18}O (p, α) ^{15}N reaction which has a resonance at 151 keV (Fig. 1). The resonance has a width of 100 eV corresponding to a depth resolution of ≈0.5 nm close to the surface [13]. As shown in Fig. 1, the as deposited sample from set A has ^{18}O only in the top layer before the thermal treatments. In contrast, set B shows contamination of 15% ^{18}O in the top $Ti^{16}O_2$ layer, probably as a consequence of diffusion occurring during sputtering deposition.

Experimentally it was verified that at room temperature the isotope composition at the surface did not change with time. In order to induce a controlled diffusion, rapid thermal annealing (RTA) was used. During this process oxygen may exchange between the surface and the atmosphere, even under a flow of inert gasses such as Ar. To prevent this exchange a capping layer of Si_3N_4, was deposited by PECVD at about 300 °C. Ellipsometry indicated a thickness of the capping layer of ≈33 nm, in agreement with ERBS measurements.

Samples from each set were exposed to temperatures between 500 and 900 °C for 5 min in an Ar atmosphere. Some samples from set B were annealed at fixed temperature of 650 °C for time periods between 5 and 100 min. After annealing, the capping layer was removed by chemical etching with solution of 6:1 BHF (6 40% NH_4F: 1 49% HF), for duration between 3 and 9 min. Etching was stopped when visual inspection made it clear that the capping layer was removed. Under high annealing temperatures Si_3N_4 changes its density and becomes more resistant to chemical etching, hence longer etching times were required. The etching process is sufficiently selective that TiO_2 removal is not an issue, as was confirmed by Rutherford Backscattering Spectrometry (RBS).

The ERBS system is described extensively elsewhere [14]. In short, electrons with 40 keV energy scatter over 135° and are energy-analyzed with a resolution of 0.3 eV. Different geometries can be used to change the depth probed. We used a perpendicular incoming ($\theta_1 = 0°, \theta_2 = 45°$) and glancing exit geometry ($\theta_1 = 35°, \theta_2 = 80°$) for bulk and surface sensitive measurements, respectively, where θ_1 and θ_2 are the incidence and exit angle with respect to the surface normal. A similar approach was previously used to determine the oxygen concentration profile for $Hf^{18}O_2/Hf^{16}O_2$ structures [9].

RBS used 2 MeV He^+ ions impinging along the surface normal and a scattered angle of 110° (i.e. detected at 70° to the sample normal). The O peak differentiation is only straight-forward for set A samples, where the energy loss in the first $Ti^{18}O_2$ layer helps separate the ^{16}O and ^{18}O peaks. Moreover, the O peaks are superimposed on the signal from the (single crystal) Si substrate. The samples were

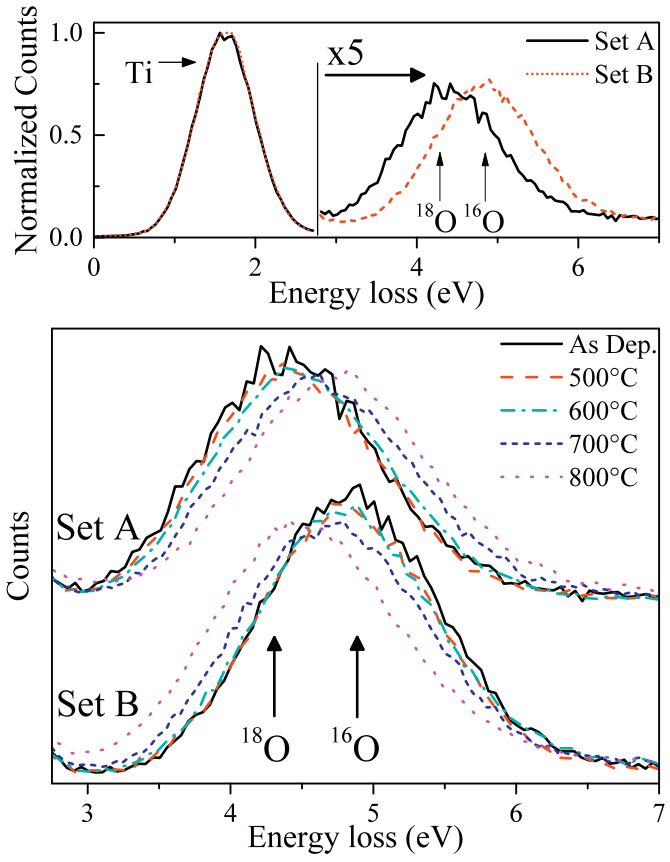

Fig. 2. The top panel shows ERBS spectra of the as deposited samples from both sets. The arrows indicate the mean, calculated energy loss for ^{16}O and ^{18}O. The spectra taken at glancing out geometry were normalized to equal Ti peak area. The lower panel shows that after thermal annealing, the O peaks shifts, indicating that some diffusion occurred.

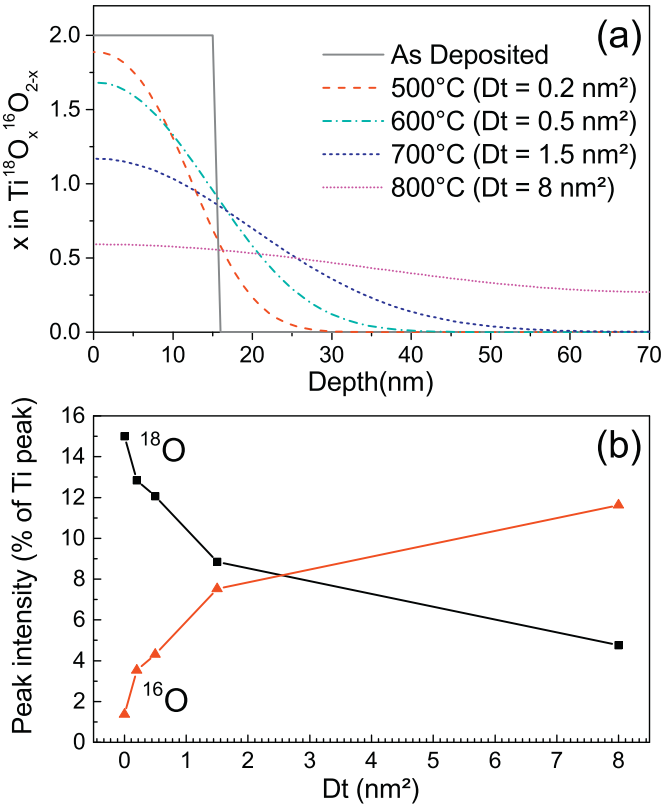

Fig. 3. In (a), diffusion profiles of samples from set A, obtained by solving the Fick's second law for different values of Dt. The ERBS peak intensity is given by the integration of the concentration profile attenuated by the length traveled by the electrons. The resultant normalized peak intensities for ^{16}O and ^{18}O are shown in (b). Thus, ERBS spectra of such samples show contributions of both ^{18}O and ^{16}O.

rotated to minimize the influence of channeling, and the Si substrate signal was subtracted to proceed with the analysis. Quantitative analysis of the O concentration profile was still difficult, so RBS spectra were analyzed based on the oxygen profiles as derived from ERBS.

4. Results and discussion

ERBS measurements of the as deposited samples in the glancing geometry are shown in Fig. 2. Under this condition, only the top layer of either $Ti^{16}O_2$ and $Ti^{18}O_2$ contributes to the spectrum. Indeed the observed O peak position depends on the isotope mass. The extra width of the O peak in the ERBS spectra due to Doppler broadening (see Eqs. (1), (2)) is resolved in the experiment. The peak width used for the fit was calculated from Eq. (2) and the same width was used before and after annealing. Then, we determined the oxide film composition from samples with thick, isotopically pure, as deposited titanium oxide layers. The sputter deposited oxide films had the expected stoichiometry of TiO_2. Subsequently, we fitted the O peaks of the sandwich structures using two components (^{16}O and ^{18}O) with the parameters as determined from the above mentioned samples. Changes in the shape of spectra could be entirely explained by variations in the intensity ratio of the ^{16}O and ^{18}O signal.

Concentration profiles were calculated by solving Fick's second law to track the ^{18}O movement, as shown in Fig. 3a. Because the stoichiometry of the oxide is TiO_2 the sum of both isotopes always equal 2, hence we may write it as $Ti^{18}O_x^{16}O_{2-x}$ and from one isotope concentration profile calculate the other. These calculations assumed that the Si substrate and the Si_3N_4 capping layer were impenetrable barriers for the oxygen. The final diffusion profile does depend on the initial concentration of ^{18}O in each layer. The result of the NRP measurements were used to determine the starting point of the Fick-diffusion profile calculation.

Once the ^{16}O and ^{18}O concentration profiles are given, the expected ERBS peak intensities for each isotope can be calculated by Eq. (4). Due to the beam attenuation, ERBS is more sensitive to the sample surface. As ^{18}O diffuses deeper, its elastic peak will become less intense. Conversely, a higher ^{16}O concentration is then found near the surface and its elastic peak becomes more intense. The complete ERBS spectrum has a superposition of elastic peaks of the two isotopes in slightly different energy positions and the relative contribution of both isotopes can be determined by fitting the spectrum. Analyzing the ratio of the ^{16}O and ^{18}O elastic peak intensities then provides a direct measure of the extent of diffusion. The resultant peak intensities for selected concentration profiles are shown in Fig. 3b.

From this analysis it is possible to determine the *Dt* values that best match the measured profiles for both ERBS geometries, as discussed before [12]. Extracted diffusion lengths, (sqrt(Dt)), and diffusion coefficients, D, are plotted in Fig. 4, as a function of annealing temperature. The diffusion coefficients are consistent for each of the two sample sets and are observed to satisfy an Arrhenius relation with an activation energy $E_A \approx 1.05$ eV.

Set A was also measured by RBS to cross check the diffusion coefficients obtained by ERBS. Fig. 5 shows the RBS spectra for different annealing temperatures, together with simulations obtained using

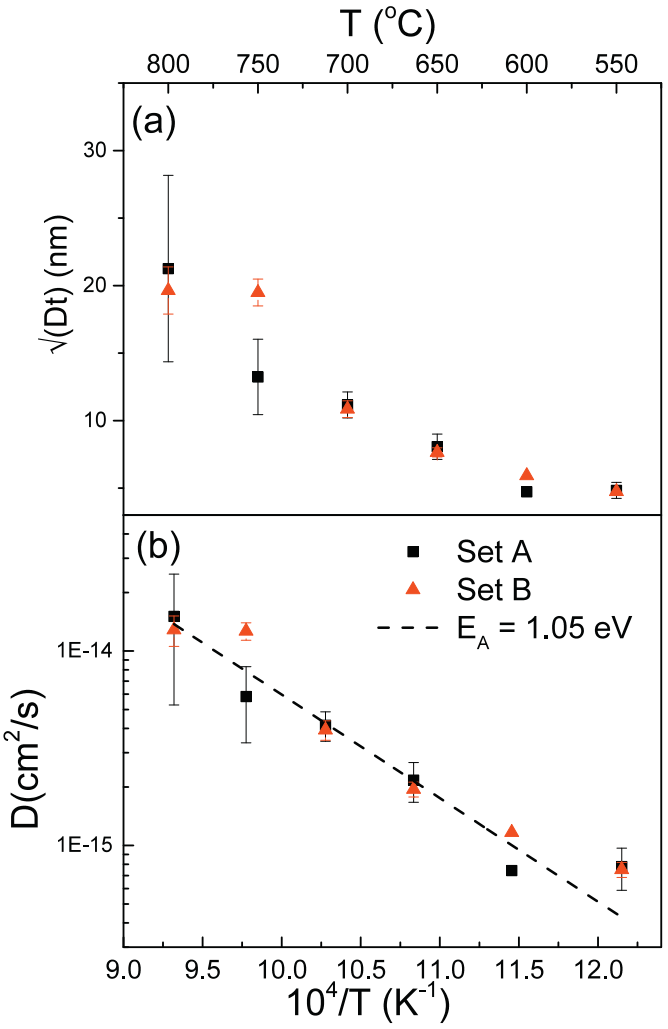

Fig. 4. Arrhenius plot for both sets. From the fitted line one can obtain the activation energy for the oxygen diffusion in TiO_2.

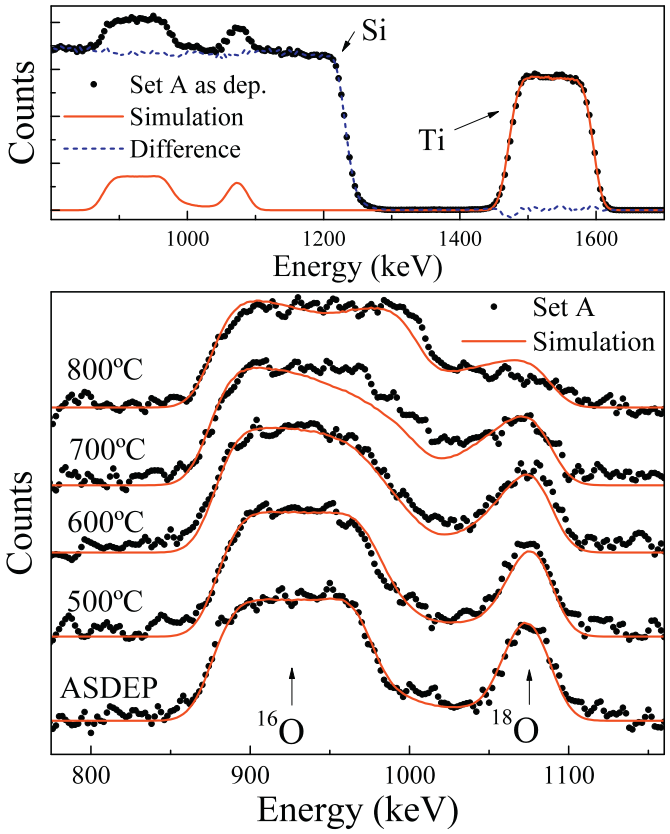

Fig. 5. The top panel shows the RBS spectrum (black points) of set *A*, as deposited sample, the red lines are simulations of the TiO_2 contribution. The difference between the experimental and simulated spectra (i.e. the Si contribution) is in blue. The bottom panel shows the oxygen region in detail (Si contribution subtracted) for different annealing temperatures.

the PowerMEIS software [15]. In a similar way to the ERBS analysis, the sample was described as a series of films of $Ti^{18}O^{16}_{2-x}O_x$ with x obtained from the Fick's diffusion profile. Quantitative analysis of the O concentration profile was still difficult, so the diffusion profiles used in these RBS simulations are those that described best the ERBS spectra. The resulting description of the RBS experiment is very good. The ERBS and RBS approaches thus describe the diffusion process consistently.

Even for single crystal rutile there is a large spread in reported activation energies [1-3,5,16,17], varying from 0.35 to 2.42 eV. The work of Arita et al. [4] follows a similar approach, where longer thermal annealings with $t > 20$ h and $T > 1000$ °C were conducted on TiO_2 samples. For the diffusion coefficients measured from set B samples, agreement is seen for similar temperatures — between 800 and 1000 °C. However, the activation energies measured are greatly different (dotted lines' slope on Fig. 6, top pane). The experiments for crystalline rutile at $T > 1000$ °C produced an activation energy of about 3 eV, which is much larger than the one obtained here for thin films of TiO_2 at lower temperatures. $E_A = 3$ eV is consistent with the diffusion of charged vacancies (V_O^{2+}) as described by ab-initio calculations from Iddir et al. [18], which estimate the vacancy forming energy and the migration energy barrier. The former is estimated at 2 eV for the given conditions, and the latter depends on the crystalline configuration, with energy barriers in different migration directions between 0.69 and 1.10 eV. These migration barriers values are consistent with the diffusion activation energy obtained here, which suggest that diffusion without thermal vacancy generation can describe our 5 min experiments but not experiments using much longer annealing time.

In order to investigate the discrepancy observed in the activation energy, further experiments were performed to determine the regularity of the diffusion. This is rather important, since previous measurements had annealing duration of a few hours instead of minutes. By keeping the annealing temperature constant at 650 °C and varying the annealing time between 5 and 100 min, diffusion lengths were measured on samples from set B. As can be observed in Fig. 6, the time dependence of the diffusion length does not follow the usual square root law expected for regular diffusion. On the contrary, two diffusion regimes may be identified. On a time scale of minutes a rapid diffusion occurs, compatible with the low activation energy measured in our samples. Then a much slower diffusion process takes place, which can be described by a larger E_A value of ≈3 eV from ref. [4].

A simplistic way to describe these experiments assumes that the sputter-deposited films have initially a high defect density. Annealing at a certain temperature will lead to their break-up resulting in diffusion of point defects. The break up of defects will be accompanied by diffusion of interstitials and vacancies. Excess point defect concentrations will increase the oxygen diffusivity, as is well known from radiation enhanced diffusion experiments. After a certain time at a given temperature the concentration of point defects will drop,

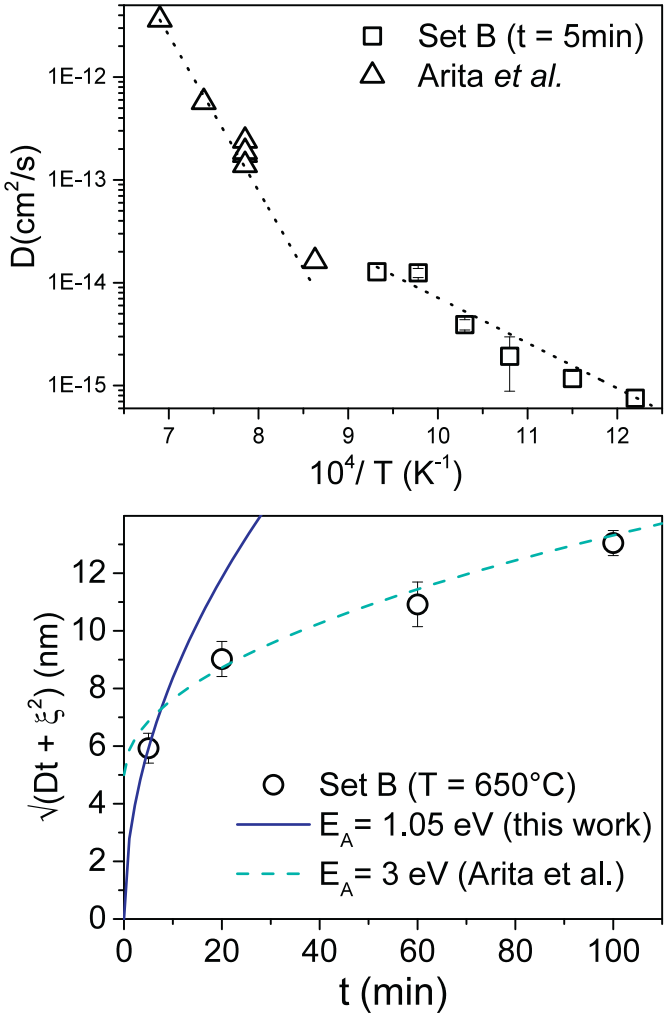

Fig. 6. On the top pane, the oxygen diffusion coefficients measured after annealing for 5 min are compared to values obtained by Arita et al. [4] for annealing with $t > 20$ h. On the bottom pane, extrapolation of the diffusion length is compared to measurements of set B samples, annealed at fixed temperature but different annealing times. The solid line corresponds to the time extrapolation using $E_A = 1.05$ eV whereas the dashed-line represents an extrapolation using $E_A = 3$ eV *and* an initial diffusion length ξ according to $\sqrt{Dt + \xi^2}$.

as only the more stable defects remain and the diffusivity will be reduced. Increasing the annealing temperature causes more defects to break up and introduces again excess point defects, increasing the diffusivity temporarily.

5. Conclusion

For the oxygen self-diffusion measurements, the electron- and ion-Rutherford backscattering techniques were employed. Particularly, ERBS was shown to have sensitivity and depth resolution required to determine the oxygen diffusion on a length scale of several 10s of nm – the length scale on which resistive switching occurs. This technique also has the advantage that it avoids possible beam damage induced diffusion during measurements. The profiles obtained by this procedure were then checked by conventional RBS measurements with 2 MeV ions. Due to the samples structure, spectra with good peak separation of the 16 and 18 isotopes were only found in one of the sample sets. Simulations, based on the profiles measured by ERBS, agree well with those measured by RBS.

Sputtered deposited samples containing $Ti^{18}O_2$ and $Ti^{16}O_2$ films were also measured with NRP, which is sensitive only to the ^{18}O isotope and is not able to probe for the total oxide stoichiometry. Therefore, the technique is useful to evaluate samples' initial conditions, however is not sufficient for a complete diffusion analysis.

The observed diffusion was found to be irregular, depending strongly on the annealing history, not just the temperature. Hence the interpretation of the experiments in terms of activation energies is questionable. However, if one interprets our 5 min isochronal annealing experiments in terms of an activation energy, one derives a value compatible with calculated oxygen vacancy migration barriers in TiO_2. Also, the sputtering deposition of TiO_2 used in our samples is known to produce films with large number of defects, condition which can enhance the initial self-diffusion rate. For longer annealing times the activation energy reported on literature is much higher than the 1.05 eV measured in the present study, indicating a slower diffusion process in which oxygen vacancy forming is necessary. Our isothermal experiments are also consistent with a transient fast diffusion process followed by a slower regime. The use of TiO_2 as oxide layer in RRAM devices is desired precisely because of this fast diffusion observed in our sputtered deposited films, even at lower annealing temperatures.

References

[1] R. Haul, G. Dumbgen, Sauerstoff-selbstdiffusion in Rutilkristallen, J. Phys. Chem. Solids 26 (1) (1965) 1–10. ISSN 0022-3697. http://www.sciencedirect.com/science/article/pii/0022369765900661. http://dx.doi.org/10.1016/0022-3697(65)90066-1.

[2] T.B. Gruenwald, G. Gordon, Oxygen diffusion in single crystals of titanium dioxide, J. Inorg. Nucl. Chem. 33 (4) (1971) 1151–1155. ISSN 0022-1902. http://www.sciencedirect.com/science/article/pii/0022190271801847. http://dx.doi.org/10.1016/0022-1902(71)80184-7.

[3] A.N. Bagshaw, B.G. Hyde, Oxygen tracer diffusion in the Magnéli phases Ti_nO_{2n-1}, J. Phys. Chem. Solids 37 (9) (1976) 835–838. ISSN 0022-3697. http://www.sciencedirect.com/science/article/pii/0022369776900585. http://dx.doi.org/10.1016/0022-3697(76)90058-5.

[4] M. Arita, M. Hosoya, M. Kobayashi, M. Someno, Depth profile measurement by secondary ion mass spectrometry for determining the tracer diffusivity of oxygen in rutile, J. Am. Ceram. Soc. 62 (9-10) (1979) 443–446. ISSN 1551-2916. http://dx.doi.org/10.1111/j.1151-_2916.1979.tb19101.x. http://dx.doi.org/10.1111/j.1151-2916.1979.tb19101.x.

[5] F. Millot, C. Picard, Oxygen self-diffusion in non-stoichiometric rutile TiO_{2x} at high temperature, Solid State Ionics 28-30 (Part 2) (1988) 1344–1348. ISSN 0167-2738. http://www.sciencedirect.com/science/article/pii/0167273888903840. http://dx.doi.org/10.1016/0167-2738(88)90384-0.

[6] X. Cui, B. Wang, Z. Wang, T. Huang, Y. Zhao, J. Yang, J.G. Hou, Formation and diffusion of oxygen-vacancy pairs on TiO_2(110)-(11), J. Chem. Phys. 129 (4). (2008) 044703. http://scitation.aip.org/content/aip/journal/jcp/129/4/10.1063/1.2955448. http://dx.doi.org/10.1063/1.2955448.

[7] X. Chen, S.S. Mao, Titanium dioxide nanomaterials: synthesis, properties, modifications, and applications, Chem. Rev. 107 (7) (2007) 2891–2959. http://dx.doi.org/10.1021/cr0500535.

[8] K. Szot, M. Rogala, W. Speier, Z. Klusek, A. Besmehn, R. Waser, TiO_2-a prototypical memristive material, Nanotechnology 22 (25). (2011) 254001. http://stacks.iop.org/0957-_4484/22/i=25/a=254001.

[9] M. Vos, P.L. Grande, D.K. Venkatachalam, S.K. Nandi, R.G. Elliman, Oxygen self-diffusion in HfO_2 studied by electron spectroscopy, Phys. Rev. Lett. 112 (2014) 175901. http://link.aps.org/doi/10.1103/PhysRevLett.112.175901. http://dx.doi.org/10.1103/PhysRevLett.112.175901.

[10] M. Vos, G.G. Marmitt, P.L. Grande, A comparison of ERBS spectra of compounds with Monte Carlo simulations, Surf. Interface Anal. (2016) n/a–n/a. http://dx.doi.org/10.1002/sia.5948. http://dx.doi.org/10.1002/sia.5948.

[11] M. Vos, R. Moreh, K. Tokeśi, The use of electron scattering for studying atomic momentum distributions: the case of graphite and diamond, J. Chem. Phys. 135 (2). (2011) 024504. http://dx.doi.org/10.1063/1.3607993.

[12] G. Marmitt, L. Rosa, S. Nandi, M. Vos, Analysis of mulit-layer ERBS spectra, J. Electron Spectrosc. Relat. Phenom. 202 (2015) 26. http://dx.doi.org/10.1016/j.elspec.2015.02.009.

[13] C. Driemeier, L. Miotti, R. Pezzi, K. Bastos, I. Baumvol, The use of narrow nuclear resonances in the study of alternative metal-oxide-semiconductor structures, Nucl. Inst. Methods Phys. Res. B 249 (1-2) (2006) 278–285. http://www.sciencedirect.com/science/article/pii/S0168583X06004599. http://dx.doi.org/10.1016/j.nimb.2006.04.013.

[14] M. Went, M. Vos, Rutherford backscattering using electrons as projectiles: underlying principles and possible applications, Nucl. Inst. Methods Phys. Res. B 266 (2008) 998–1011. http://dx.doi.org/10.1016/j.nimb.2008.01.059.

[15] M.A. Sortica, P.L. Grande, G. Machado, L. Miotti, Characterization of nanoparticles through medium-energy ion scattering, J. Appl. Phys. 106 (11). (2009) http://dx.doi.org/10.1063/1.3266139.
[16] J. Nowotny, T. Bak, M.K. Nowotny, L.R. Sheppard, Chemical diffusion in metal oxides. Example of TiO_2, Ionics 12 (3) (2006) 227–243. http://dx.doi.org/10.1007/s11581-006-0036-0.
[17] D. Derry, D. Lees, J. Calvert, A study of oxygen self-diffusion in the C-direction of rutile using a nuclear technique, J. Phys. Chem. Solids 42 (1) (1981) 57–64. http://dx.doi.org/10.1016/0022-3697(81)90011-1.
[18] H. Iddir, S. Öğüt, P. Zapol, N.D. Browning, Diffusion mechanisms of native point defects in rutile TiO_2: *ab initio* total-energy calculations, Phys. Rev. B 75 (2007) 073203. http://link.aps.org/doi/10.1103/PhysRevB.75.073203. http://dx.doi.org/10.1103/PhysRevB.75.073203.